Price-based Demand Response Supported Three-stage Hierarchically Coordinated Voltage Control for Microgrids

Bo Wang, *Member*, *IEEE*, Cuo Zhang, *Senior Member*, *IEEE*, Xingying Chen, *Senior Member*, *IEEE*, Yan Xu, *Senior Member*, *IEEE*, Kun Yu, *Senior Member*, *IEEE*, Haochen Hua, *Member*, *IEEE*, and Zhao Yang Dong, *Fellow*, *IEEE*

***Abstract*—Photovoltaic (PV) inverter, as a promising voltage/var control (VVC) resource, can supply flexible reactive power to reduce microgrid power loss and regulate bus voltage. Meanwhile, active power plays a significant role in microgrid voltage profile. Price-based demand response (PBDR) can shift load demand via determining time-varying prices, which can be regarded as an effective means for active power shifting. However, due to the different characteristics, PBDR and inverter-based VVC lack systematic coordination. Thus, this paper proposes a PBDR-supported three-stage hierarchically coordinated voltage control method, including day-ahead PBDR price scheduling, hour-ahead reactive power dispatch of PV inverters, and real-time local droop control of PV inverters. Considering their mutual influence, a stochastic optimization method is utilized to centrally or hierarchically coordinate adjacent two stages. To solve the bilinear constraints of droop control function, the problem is reformulated into a second-order cone programming relaxation model. Then, the concave constraints are convexified, forming a penalty convex-concave model for feasible solution recovery. Lastly, a convex-concave procedure-based solution algorithm is proposed to iteratively solve the penalty model. The proposed method is tested on 33-bus and IEEE 123-bus distribution networks and compared with other methods. The results verify the high efficiency of the proposed method to achieve power loss reduction and voltage regulation.**

***Index Terms*—Photovoltaic inverter, voltage control, demand response, convex-concave procedure, second-order cone programming relaxation.**

Manuscript received: March 11, 2024; revised: April 6, 2024; accepted: May 28, 2024. Date of CrossCheck: May 28, 2024. Date of online publication: Jun. 25, 2024.

This work was supported in part by the National Natural Science Foundation of China (No. 52307091), in part by the Natural Science Foundation of Jiangsu Province (No. BK20230952), in part by the China Postdoctoral Science Foundation (No. 2023M740976), and in part by the Start Up Grant of City University of Hong Kong (No. 9380163).

B. Wang (corresponding author), X. Chen, K. Yu, and H. Hua are with the School of Electrical and Power Engineering, Hohai University, Nanjing 211100, China (e-mail: bowangee@hhu.edu.cn; xychen@hhu.edu.cn; kunyu@hhu.edu.cn; huahc16@tsinghua.org.cn).

C. Zhang is with the School of Electrical and Computer Engineering, The University of Sydney, Sydney, NSW 2006, Australia (e-mail: cuo.zhang@sydney.edu.au).

Y. Xu is with the Center for Power Engineering (CPE), School of Electrical and Electronic Engineering, Nanyang Technological University, Singapore 639798, Singapore (e-mail: eeyanxu@gmail.com).

Z. Y. Dong is with the Department of Electrical Engineering, City University of Hong Kong, Hong Kong, China (e-mail: zydong@ieee.org).

DOI: 10.35833/MPCE.2024.000263

NOMENCLATURE

A. Sets and Indices

B	Set of branches ij
$f_m(\cdot)$, $g_m(\cdot)$	Convex functions
h, i, j	Indices of microgrid buses
$H(i)$	Set of parent buses of bus i
I	Set of microgrid buses
$J(i)$	Set of child buses of bus i
k	Index of iterations
L, l	Set and index of price levels of price-based demand response (PBDR)
m	Index of objective function and constraints, starting from 0
S, s	Set and index of sampled scenarios
T, t, τ	Set, index, and length of time intervals
v	Index of regular dodecagon vertices

B. Parameters

ε	Price elasticity of loads
ω	Weighting factor
$\pi^{\max}$	The maximum penalty factor
π^k	Penalty factor at iteration k
$\underline{(\cdot)}$, $\overline{(\cdot)}$	Lower and upper bounds
$\widetilde{(\cdot)}$, $\widehat{(\cdot)}$	Uncertainty and expected value of uncertainty
$(\cdot)^*$	Obtained result of decision variable
A_v, B_v, C_v	Coefficients of dodecagon inner approximation
C^{Pr}	Coefficient of electricity price
$\boldsymbol{D}$, $\boldsymbol{E}$	Coefficient matrices of day-ahead and intra-day decision variables
L_l	Demand response rate at price level l (%)
N_i, N_s	Total numbers of buses and scenarios
$Pr_{l,t}$	Price level of PBDR ($/MWh)

Pr_0	Electricity price before PBDR ($/MWh)
$Q_{i,t}^{\max}$	The maximum reactive power generation of photovoltaic (PV) inverter (kvar)
r_{ij}, x_{ij}	Resistance and reactance of branch *ij* (p.u.)
$S_{ij}^{\max}$	The maximum capacity of branch (kVA)
$V^{\max}$	The maximum bus voltage (p.u.)
$V^{\min}$	The minimum bus voltage (p.u.)

C. Variables

$\alpha_{l,t}$	Binary decision of price level of PBDR
β_i	Binary decision of slope of droop control function
λ_i	Slope of droop control function
$P_{ij,t}, Q_{ij,t}$	Active and reactive power flows through branch *ij* (kW and kvar)
$P_{ij,t}^{loss}$	Power loss of branch *ij* (kW)
$P_{i,t}^{PV}$	Active power generation of PV (kW)
$P_{i,t}^{LD}, Q_{i,t}^{LD}$	Active and reactive power of load demand without PBDR (kW and kvar)
$P_{i,t}^{LD_P}, Q_{i,t}^{LD_P}$	Active and reactive power of load demand with PBDR implemented (kW and kvar)
$Q_{i,t}^{set}$	Reactive power setpoint of inverter (kvar)
$Q_{i,t}^{inv}$	Reactive power output of inverter (kvar)
$\Delta Q_{i,t}$	Reactive power adjustment of inverter responding to voltage variation (kvar)
$s_{1,i,t}, s_{2,i,t}$	Relaxation errors
$\Delta V_{i,t}$	Voltage variation from expected voltage value (p.u.)
$V_{i,t}$	Bus voltage (p.u.)
V_0	Reference voltage (p.u.)
$V_{i,t}^{exp}$	Expected bus voltage in expected scenario of uncertainties (p.u.)
V_t^{dev}	Average bus voltage deviation (p.u.)
$\boldsymbol{x} \in \mathbf{R}^n$	Vector of decision variables in convex-concave procedure

I. Introduction

SOLAR photovoltaic (PV) units have been growingly installed in microgrids. However, the high penetration of PV may cause voltage issues such as voltage rise [1] and voltage fluctuation [2], posing a significant threat to microgrid operation, due to the supply-demand mismatch and the stochastic output of PV [3]. Also, the infrastructure upgrade and PV active power curtailment are not cost-effective ways to improve the microgrid operation profiles.

To conquer this challenge, voltage/var control (VVC) is an effective measure that can reduce network power loss or regulate bus voltage. Conventional mechanical VVC resources, including capacitor banks (CBs) and transformer on-load tap changers (OLTCs), operate in a discontinuous manner and thus cannot respond to voltage fluctuation timely [4]. In practice, not all microgrids are equipped with these VVC devices. Alternatively, with the proliferation of distributed PV generation, smart PV inverters can produce continuous reactive power with fast response speed [2], [4]. Also, the PV inverter is oversized, such that additional reactive power can be generated during the peak PV period [5]. As a result, the PV inverter has been recommended by IEEE Std 1547 working group for VVC function [6].

Generally, the VVC method can be categorized into central control and local control. As implied by the name, the former optimizes the operating decisions of VVC resources based on several global information including the prediction of renewable generation and load demand as well as network parameters. In [7], a two-stage chance-constrained VVC approach is given to minimize the network power loss. The dispatch decisions of CBs, OLTC, and voltage regulators are determined in the first stage, while the reactive power generation of inverters is optimized in the second stage. Reference [8] proposes a distributed robust VVC method based on the network partition. Moreover, the reactive power compensation of the inverter is utilized to address the voltage rise issue, which in turn enhances the solar hosting capacity of distribution networks [9]. Network reconfiguration is coordinated with voltage control resources to improve the voltage profile of network operation [10]. An electric spring-based multi-objective voltage control method considering power flow is proposed. The nonlinear model is solved by a continuous genetic algorithm [11]. However, these central VVC methods focus on optimizing the operation setpoints of the VVC devices over a specific time interval and thus cannot track the real-time (RT) variation of the stochastic renewable generation and load demand.

Alternatively, the local VVC device responds to the local measurement such as bus voltage based on the built-in control strategy. In [12], a two-layer local RT adaptive VVC approach is developed to optimize a *Q-V* droop control function, aiming to achieve low steady-state error and control stability by PV inverters. The high efficiency of voltage-dependent VVC has been verified by [13]. However, since only the local information is used, the local VVC method can hardly achieve a system-wide optimum.

Recently, the integration of the central and local VVC methods has drawn more attention. The parameters of local droop control functions such as droop slope are optimized simultaneously with the central VVC decisions based on the system-wide information, forming a hierarchical VVC framework. In [2], the reactive power setpoint and voltage intercept of a linear *Q-V* droop control function are determined at the central VVC level with a pre-set droop slope. Then, a *Q-V* droop model is further proposed considering the optimization of droop slope, but the model is nonlinear [14]. Furthermore, the *P-V* and *Q-V* droop control functions of inverters are co-optimized in [15]. Similar to [2], the droop slopes are assumed to be determined in advance. In [16], a two-timescale energy management method with multi-terminal soft open points is proposed. The slope of the linear droop control function is optimized based on a pre-determined reference setpoint, which introduces bilinear terms and thus may reduce computation efficiency. Moreover, the OLTC, CB,

and PV inverters are coordinated in [17] through a multi-timescale reactive power dispatch approach. The *Q*-*P* droop control function of PV inverters is optimized using an islanded affine robust optimization method. Reference [18] divides the droop control function into several pieces and optimizes them separately. Similarly, the nonlinear model and newly introduced binary variables could increase computation burdens. References [19] and [20] also apply piecewise modelling approaches to describe the droop control function. To make the droop control function model linear, some parameters such as voltage setpoints corresponding to droop inflection points are pre-set before the optimization. In addition, the optimizations of *P*-*f* and *Q*-*V* droop control functions are studied in the islanded mode of microgrids. In [21], the droop control functions with pre-set droop gain are considered to promote the hosting capacity of renewable energy in islanded microgrids. Moreover, [22] proposes a stagewise droop parameter optimization method for isolated microgrids considering operation safety constraints. The droop control function is modelled nonlinearly and optimized in the first stage, after which partial droop parameters can be adjusted in the second and third stages. From the above literature, the droop control functions are either modelled in a nonlinear manner, leading to a heavy computation burden, or simplified with the pre-determination of certain key droop parameters.

In addition, except for reactive power, active power also plays an important role in microgrid voltage profiles and power losses during operation. Price-based demand response (PBDR) is a typical demand response scheme that aims to encourage users to shift their partial electricity consumption via scheduling time-varying prices [23]. Unlike distributed energy resources such as microturbines and battery energy storage devices, PBDR does not require additional operating costs. Furthermore, considering that microgrid operators could have the retailer attribute [24], [25], different PBDR prices can be scheduled to achieve load leveling and shifting, which in turn affects microgrid voltage profiles and power losses. In [26], a stepwise PBDR is designed to coordinate with battery energy storage, aiming to achieve the economic operation of microgrids. Moreover, PBDR is considered in a two-stage robust model for distributed generation allocation [27]. PBDR is also integrated into a dispatch and bidding strategy of virtual power plants [28].

However, most existing PBDR-related research works focus on cost minimization, and the linkage between PBDR and grid voltage control in the microgrid is often ignored. Moreover, the PBDR prices are generally scheduled in advance, giving users sufficient time for response, while the inverter reactive power is managed at a short time interval. Therefore, based on their different characteristics, a multi-stage hierarchical framework is required to systematically coordinate PBDR with VVC.

Through the above literature review, it can be found that droop control functions are either modelled with the pre-determined parameters, or modelled in a nonlinear manner that requires an efficient solving method. Also, a multi-stage hierarchical framework is needed to coordinate PBDR and inverter-based VVC for microgrid operation. To bridge the research gap, this paper proposes a PBDR-supported three-stage hierarchically coordinated voltage control (HCVC) method. To efficiently optimize the droop control function with the bilinear constraints, a convex-concave procedure (CCP) [29] based solution algorithm is developed. Thus, the main contributions of this paper are given as follows:

1) A PBDR-supported three-stage HCVC method is proposed to efficiently coordinate the PBDR and inverter-based VVC resources at different hierarchies and timescales, aiming to minimize the microgrid power loss and voltage deviation. The droop slope and a pair of base coordinates consisting of the expected bus voltage and reactive power setpoint are fully modelled, such that the key parameters of the local *Q*-*V* droop control function can be integrated into the central hierarchy for intraday optimization.

2) To address the bilinear constraints of droop control function model in the second-stage hierarchical VVC, a second-order conic relaxation (SOCR) model is introduced. Then, considering the relaxation errors, a penalty convex-concave model is proposed to reformulate and convexify the relaxed constraints. Accordingly, a CCP-based solution algorithm is developed to efficiently solve the second-stage optimization.

II. Coordinated Framework of PBDR and Inverter-based VVC

A PBDR-supported three-stage HCVC method is proposed to minimize microgrid power loss and voltage deviation by co-optimizing the operation of both active and reactive power resources. Its framework is illustrated in Fig. 1. The first and second stages belong to the central layer managed by a central optimizer using system-wide information. By contrast, the third stage belongs to the local VVC layer implemented by the local controller of each PV inverter using local RT voltage measurement.

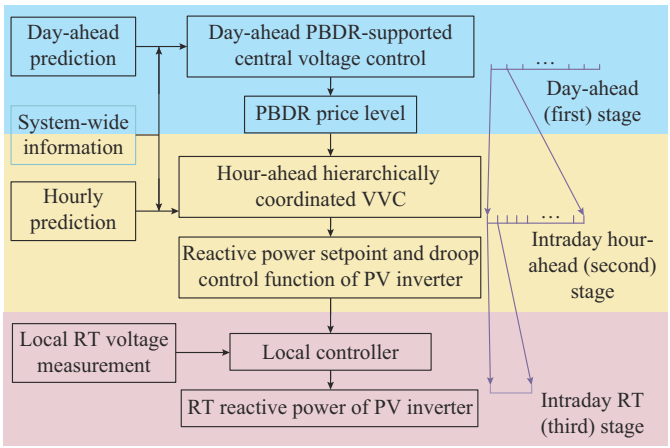

Fig. 1. Framework of proposed PBDR-supported three-stage HCVC method.

In the first stage, with the day-ahead prediction of PV outputs and loads, the day-ahead PBDR prices are determined and scheduled for load shifting, aiming to achieve peak shaving and valley filling. These prices are scheduled one day ahead in order to give consumers enough response time.

Moreover, the intraday hour-ahead reactive power dispatch of PV inverters is taken into account under uncertainties in this stage, forming central coordination between the first and second stages.

Then, with more accurate hourly prediction of PV outputs and loads, the second stage optimizes the parameters of the *Q-V* droop control functions as well as reactive power setpoints of PV inverters on an hourly basis. The results are delivered to the corresponding PV inverters for the local VVC. Since the system-wide information and possible scenarios of uncertainty realizations are used to determine the droop control functions, it hierarchically coordinates the central and local layers.

Lastly, in the third stage, with the local RT voltage measurement, PV inverters generate RT reactive power based on the optimized setpoint and droop control functions. In other words, inverters can generate either constant or dynamic reactive power based on the optimized droop control function.

It is worth noting that as the size and scale of the microgrid increase, the three-phase unbalance issue becomes gradually evident. This could be tackled by scheduling PBDR price levels and optimizing PV reactive power generation on the basis of each phase.

III. Day-ahead Central Coordination of PBDR and VVC

A. PBDR

The purpose of PBDR is to motivate users to shift their partial electricity loads by scheduling different hourly prices one day ahead. A high price will encourage consumers to reduce their load demand and vice versa. Since there is a strong connection between load demand and network bus voltage or power loss, it is expected to increase the load during the peak PV generation period and decrease the load during the peak load period.

According to [30], the relationship between electricity price Pr^{ε} and load demand P^{LD} can be formulated as:

$$P^{LD} = C^{Pr} \cdot Pr^{\varepsilon} \tag{1}$$

To efficiently implement PBDR, five price levels are designed based on (1), forming a stepwise price-elastic demand model [26]. The designed stepwise PBDR price levels in this paper are given in Table I.

TABLE I
Designed Stepwise PBDR Price Levels

Price level	Price rate (%)	Demand response rate L_l (%)
1	60	121
2	80	108
3	100	100
4	130	93
5	170	88

By setting different price levels, the microgrid load demand is expected to change accordingly. Thus, the active and reactive power of the loads with PBDR can be modelled as:

$$\tilde{P}_{i,t}^{LD_p} = \tilde{P}_{i,t}^{LD} \sum_{l \in L} \alpha_{l,t} L_l \quad \forall t \tag{2}$$

$$\tilde{Q}_{i,t}^{LD_p} = \tilde{Q}_{i,t}^{LD} \sum_{l \in L} \alpha_{l,t} L_l \quad \forall t \tag{3}$$

It is worth noting that the load uncertainties such as prediction errors and non-responsive loads can be considered in $\tilde{P}_{i,t}^{LD}/\tilde{Q}_{i,t}^{LD}$ and $\tilde{P}_{i,t}^{LD_p}/\tilde{Q}_{i,t}^{LD_p}$. Other constraints for PBDR implementation are given as:

$$\sum_{l \in L} \alpha_{l,t} = 1 \quad \forall t \tag{4}$$

$$\sum_{t \in T} \sum_{i \in I} \sum_{l \in L} (Pr_{l,t} \cdot \tilde{P}_{i,t}^{LD} \alpha_{l,t} L_l \tau) \le \sum_{t \in T} \sum_{i \in I} (Pr_0 \cdot \tilde{P}_{i,t}^{LD} \tau) \tag{5}$$

$$\sum_{t \in T} \sum_{i \in I} \sum_{l \in L} \tilde{P}_{i,t}^{LD} \alpha_{l,t} L_l \tau \ge \sum_{t \in T} \sum_{i \in I} \tilde{P}_{i,t}^{LD} \tau \tag{6}$$

$$\sum_{i \in I} \sum_{l \in L} \tilde{P}_{i,t}^{LD} \alpha_{l,t} L_l \tau \le \max\left(\sum_{i \in I} \tilde{P}_{i,t}^{LD} \tau \right) \quad \forall t \tag{7}$$

where τ is set to be 1 hour in the day-ahead stage.

Constraint (4) ensures that only one price level of PBDR can be activated every hour. Constraint (5) indicates that the consumers' electricity bills with the scheduled PBDR cannot be greater than their original bills. Constraint (6) states that the consumers' electricity consumption should not be compromised by PBDR. Lastly, the total hourly load after PBDR is constrained by (7), indicating that a new peak load cannot be created.

The above PBDR implementation is used to achieve load shifting from the perspective of the microgrid system by scheduling different PBDR price levels. The uncertainties of loads will be further addressed by a stochastic optimization (SO) in Section III-C.

B. Day-ahead PBDR-supported Central Voltage Control Model

The day-ahead PBDR-supported central voltage control coordinately optimizes the PBDR scheduling and inverter reactive power dispatch to achieve the reduction of microgrid power loss and voltage deviation. This day-ahead model is formulated as:

$$\min\left(\omega \sum_{t \in T} \sum_{ij \in B} P_{ij,t}^{loss} + (1-\omega) \sum_{t \in T} V_t^{dev} \right) \tag{8}$$

s.t.

(2)-(7)

$$-Q_{i,t}^{\max} \le Q_{i,t}^{inv} \le Q_{i,t}^{\max} \quad \forall i, \forall t \tag{9}$$

$$\sum_{h \in H(i)} P_{hi,t} = \sum_{j \in J(i)} P_{ij,t} - \tilde{P}_{i,t}^{PV} + \tilde{P}_{i,t}^{LD_p} \quad \forall h, \forall i, \forall j, \forall t \tag{10}$$

$$\sum_{h \in H(i)} Q_{hi,t} = \sum_{j \in J(i)} Q_{ij,t} - Q_{i,t}^{inv} + \tilde{Q}_{i,t}^{LD_p} \quad \forall h, \forall i, \forall j, \forall t \tag{11}$$

$$V_{j,t} = V_{i,t} - \frac{P_{ij,t} r_{ij} + Q_{ij,t} x_{ij}}{V_0} \quad \forall i, \forall j, \forall t \tag{12}$$

$$V_t^{dev} = \frac{1}{N_i} \sum_{i \in I} \frac{\left| V_{i,t} - V_0 \right|}{V_0} \quad \forall t \tag{13}$$

$$P_{ij,t}^{loss}=r_{ij}\frac{P_{ij,t}^2+Q_{ij,t}^2}{V_0^2}\quad \forall ij,\forall t \tag{14}$$

$$V^{\min}\le V_{i,t}\le V^{\max}\quad \forall i,\forall t \tag{15}$$

$$P_{ij,t}^2+Q_{ij,t}^2\le(S_{ij}^{\max})^2\quad \forall ij,\forall t \tag{16}$$

The objective function (8) minimizes the total microgrid power loss and average bus voltage deviation with the assigned weighting factor ω. The PBDR-related constraints can be referred to (2)-(7). Furthermore, (9) constrains the inverter reactive power supply. $Q_{i,t}^{\max}$ can be calculated first based on the predicted PV generation and inverter settings. Note that even though the rated active power is output, the PV inverters can still generate extra reactive power [5]. Equations (10)-(12) denote the linearized Dist-flow model [31]. The average bus voltage deviation and branch power loss are calculated by (13) and (14), respectively. The bus voltage and branch apparent power are restricted by (15) and (16), respectively.

To efficiently solve the day-ahead model, some constraints can be further linearized. Firstly, the absolute expression $|A-B|$ in (13) can be linearized by introducing a slack variable C. Thus, the absolute expression can be reformulated as $C\ge A-B$ and $C\ge B-A$, and the objective function will minimize C instead of $|A-B|$.

Secondly, the quadratic inequality in (16) is linearized by a polygonal inner approximation approach [32], as shown in Fig. 2.

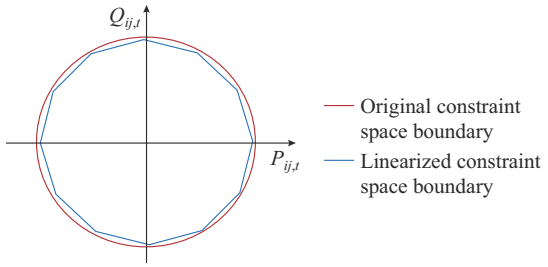

Fig. 2. Illustration of polygonal inner approximation approach using a regular dodecagon.

The feasible region formed by active and reactive power is approximated by a regular polygon. A regular dodecagon is used in this paper. Based on the coordinates of vertices, (16) can be converted into the following forms:

$$A_vP_{ij,t}+B_vQ_{ij,t}\le C_v(S_{ij}^{\max})^2\quad \forall ij,\forall t,\forall v\in\{1,2,\ldots,12\} \tag{17}$$

With the above linearization approaches, the day-ahead PBDR-supported central voltage control model including (2)-(15), (17) forms a mixed-integer quadratic programming problem. The primary decision variables are $\alpha_{l,t}$ and $Q_{i,t}^{inv}$, and the uncertainties include $\tilde{P}_{i,t}^{PV}$ and $\tilde{P}_{i,t}^{LD}$.

C. SO for Uncertainties

To address the uncertainties of the PV outputs and loads, a scenario-based SO method [33] is applied. In this method, multiple scenarios are randomly generated based on the probability distribution of the uncertainties to represent the possible uncertainty realizations. Considering that the probability distribution could be unknown or inaccurate, a sample average approximation method [34] is used in this paper. Thus, the stochastic programming model of the proposed day-ahead PBDR-supported central voltage control can be formulated as the following compact matrix form:

$$\min_{x}\ \boldsymbol{D}x+\min_{y_s}\frac{1}{N_s}\sum_{s\in S}\boldsymbol{E}y_s \tag{18a}$$

s.t.

$$(2)\text{-}(7),\ (9)\text{-}(15),\ (17)\quad \forall i,\forall j,\forall t,\forall s \tag{18b}$$

$$\begin{cases}P_{i,t,s}^{PV}\in S\\ P_{i,t,s}^{LD}\in S\end{cases} \tag{18c}$$

where x denotes the day-ahead decision variable $\alpha_{l,t}$; and y_s denotes the intraday decision variables including $Q_{i,t}^{inv}$ and other dependent variables in scenario s.

It is noteworthy that after solving (18), only $\alpha_{l,t}^{*}$ is scheduled and $Q_{i,t}^{inv}$ will be re-optimized in the intraday stage according to more accurate hourly predictions.

IV. Hour-ahead Hierarchically Coordinated VVC

A. Inverter Reactive Power Generation with Local Droop Control

The inverter reactive power output can be fixed at the setpoint or adjusted based on the droop control function. Thus, this dual output mode is considered in the inverter reactive power generation.

The conventional Q-V droop control function embedded in the PV inverter is illustrated in Fig. 3(a). According to this droop curve, the inverter produces a constant reactive power Q_i^{base} when the magnitude of the local bus voltage is inside a deadband $\left[\underline{V}_i^{DB},\overline{V}_i^{DB}\right]$. Besides, the inverter adjusts its reactive power based on the droop control function if the magnitude of the local bus voltage is out of the deadband.

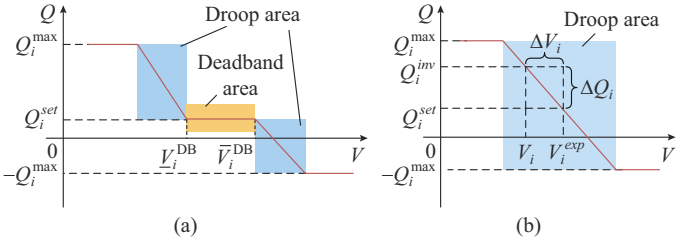

Fig. 3. Conventional Q-V droop control function and linear droop control function. (a) Conventional Q-V droop control function. (b) Linear droop control function.

However, when the bus voltage stays inside the deadband, the inverter does not react to the system variation, resulting in inadequate utilization of the inverter reactive power capacity. To make full use of inverter reactive power capacity, a linear droop control function is employed [2], as illustrated in Fig. 3(b). Thus, the inverter reactive power output is formulated as:

$$Q_{i,t}^{inv}=Q_i^{set}+\Delta Q_{i,t}\quad \forall i,\forall t \tag{19}$$

$$\Delta V_{i,t}=V_{i,t}-V_i^{exp}\quad \forall i,\forall t \tag{20}$$

$$\Delta Q_{i,t}=\lambda_i \Delta V_{i,t} \quad \forall i,\forall t \tag{21}$$

$$\beta_i \underline{\lambda} \le \lambda_i \le \beta_i \overline{\lambda} \quad \forall i \tag{22}$$

$$\begin{cases} -Q_{i,t}^{\max} \le Q_i^{set} \le Q_{i,t}^{\max} \\ -Q_{i,t}^{\max} \le Q_{i,t}^{inv} \le Q_{i,t}^{\max} \end{cases} \quad \forall i,\forall t \tag{23}$$

where the subscript t denotes the index of RT time interval in the hour-ahead stage.

The droop control function of the inverter is described by (19) - (23). Equation (19) calculates the RT reactive power supply consisting of a reactive power setpoint and a RT reactive power adjustment. Then, the difference between RT bus voltage $V_{i,t}$ and expected bus voltage V_i^{exp} is calculated by (20). Equation (21) states that the reactive power adjustment in response to the voltage variation is based on the slope of droop control function, which is further limited by (22). Note that if β_i is zero, the inverter will generate a constant reactive power at Q_i^{set}. Finally, the inverter reactive power output and setpoint are constrained by (23). It can be observed that the variables λ_i, V_i^{exp}, Q_i^{set} and the parameter $Q_{i,t}^{\max}$ make up the linear droop control function.

B. Hour-ahead Hierarchically Coordinated VVC Model

Based on the inverter reactive power generation, the hour-ahead hierarchically coordinated VVC is modelled as:

$$obj_0: \min\left(\omega \sum_{t\in T}\sum_{ij\in B} P_{ij,t}^{loss} + (1-\omega)\sum_{t\in T} V_t^{dev}\right) \tag{24a}$$

s.t.

$$(2)-(3),(10)-(15),(17),(19)-(23) \tag{24b}$$

Considering more accurate hour-ahead prediction of PV generation and loads, i.e., these uncertainties will be realized in a shorter predicted time interval, the SO method is applied to simulate the RT uncertainty realization through scenario generation. The slope of droop control function λ_i, reactive power setpoint Q_i^{set}, and the corresponding expected bus voltage V_i^{exp} are optimized in the generated scenarios. It is noted that this hour-ahead model (24) is nonlinear due to the bilinear term in (21), which will be addressed in the following subsections.

C. CCP-based Reformulation

The bilinear term in (21) significantly decreases the solving efficiency. To solve this problem, firstly, (21) is converted into a SOCR model, offering an initial approximate solution. Then, a penalty CCP model is introduced to recover a feasible solution.

1) SOCR Model

For illustration, the subscripts are temporally neglected at this stage. The bilinear term can be converted into an equivalent form, shown as:

$$\lambda \Delta V = \Delta Q = z_1 - z_2 \tag{25a}$$

$$\begin{cases} z_1 = \left(\dfrac{\lambda+\Delta V}{2}\right)^2 \\ z_2 = \left(\dfrac{\lambda-\Delta V}{2}\right)^2 \end{cases} \tag{25b}$$

Then, the quadratic equality constraint (25b) can be reformulated as:

$$\begin{cases} z_1 \ge \left(\dfrac{\lambda+\Delta V}{2}\right)^2 \\ z_2 \ge \left(\dfrac{\lambda-\Delta V}{2}\right)^2 \end{cases} \tag{26a}$$

$$\begin{cases} z_1 \le \left(\dfrac{\lambda+\Delta V}{2}\right)^2 \\ z_2 \le \left(\dfrac{\lambda-\Delta V}{2}\right)^2 \end{cases} \tag{26b}$$

Constraint (26a) is convex while constraint (26b) is concave. Multiplying both sides of (26a) by 4, it can be rewritten into a second-order cone form, given as:

$$\left\| \begin{matrix} \lambda+\Delta V \\ 1-z_1 \end{matrix} \right\|_2 \le 1+z_1 \tag{27a}$$

$$\left\| \begin{matrix} \lambda-\Delta V \\ 1-z_2 \end{matrix} \right\|_2 \le 1+z_2 \tag{27b}$$

Lastly, the concave (26b) is removed and a McCormick envelope [35] is added to tighten this relaxation, as shown in (28).

$$\Delta Q \ge \underline{\lambda}\Delta V + \lambda \underline{\Delta V} - \underline{\lambda}\,\underline{\Delta V} \tag{28a}$$

$$\Delta Q \ge \overline{\lambda}\Delta V + \lambda \overline{\Delta V} - \overline{\lambda}\,\overline{\Delta V} \tag{28b}$$

$$\Delta Q \le \overline{\lambda}\Delta V + \lambda \underline{\Delta V} - \overline{\lambda}\,\underline{\Delta V} \tag{28c}$$

$$\Delta Q \le \underline{\lambda}\Delta V + \lambda \overline{\Delta V} - \underline{\lambda}\,\overline{\Delta V} \tag{28d}$$

Thus, by replacing (21) with (25a), (27), and (28), the original hour-ahead problem forms a SOCR model. It is noted that, since the objective function is not strictly increasing in λ_i and $\Delta V_{i,t}$, this SOCR model is not exact and it only provides a lower bound to the original problem.

2) Penalty Convex-concave Model

The above SOCR model is loose for the bilinear term and may cause relaxation errors, because constraint (27) is only restricted on one side. To address this issue, a CCP-based reformulation is proposed to transfer the SOCR model into a penalty convex-concave model by convexifying the concave constraints. The original CCP is introduced to seek the solution to the difference of convex programming problems [36], which is briefly introduced below.

$$\min(f_0(\boldsymbol{x}) - g_0(\boldsymbol{x})) \tag{29a}$$

s.t.

$$f_m(\boldsymbol{x}) - g_m(\boldsymbol{x}) \le 0 \quad \forall m \tag{29b}$$

It is noted that $-g_m(\boldsymbol{x})$ is concave. This concave term is replaced by a convex upper bound, which obtains the following problem.

$$\min(f_0(\boldsymbol{x}) - \dot{g}_0(\boldsymbol{x}, \boldsymbol{x}^{k^*})) \tag{30a}$$

s.t.

$$f_m(\boldsymbol{x}) - \dot{g}_m(\boldsymbol{x}, \boldsymbol{x}^{k^*}) \le 0 \quad \forall m \tag{30b}$$

$$\dot{g}_m(\boldsymbol{x}, \boldsymbol{x}^{k^*}) = g_m(\boldsymbol{x}^{k^*}) + \nabla g_m(\boldsymbol{x}^{k^*})^{\mathrm{T}}(\boldsymbol{x} - \boldsymbol{x}^{k^*}) \quad \forall m \tag{30c}$$

where $\dot{g}_m(\boldsymbol{x},\boldsymbol{x}^{k*})$ is the linearized function of $g_m(\boldsymbol{x})$, which can be regarded as a tangent plane of $g_m(\boldsymbol{x})$, at the current solution point $\boldsymbol{x}^{k*}$. As a result, this linearized model (30) can be solved iteratively to obtain the solution.

In line with the form of (30), the concave (26b) can be reformulated into the difference between $z_{1/2}$ and $\dot{g}_{1/2}(\lambda,\Delta V)$, as shown in (31).

$$z_1-\dot{g}_1(\lambda,\Delta V)\le 0 \tag{31a}$$

$$\dot{g}_1(\lambda,\Delta V)=\frac{\lambda^{k*}+\Delta V^{k*}}{2}(\lambda+\Delta V)-\left(\frac{\lambda^{k*}+\Delta V^{k*}}{2}\right)^2 \tag{31b}$$

$$z_2-\dot{g}_2(\lambda,\Delta V)\le 0 \tag{31c}$$

$$\dot{g}_2(\lambda,\Delta V)=\frac{\lambda^{k*}-\Delta V^{k*}}{2}(\lambda-\Delta V)-\left(\frac{\lambda^{k*}-\Delta V^{k*}}{2}\right)^2 \tag{31d}$$

Since the relaxation errors need to be reduced, slack variables are introduced to represent the difference, as given in (32).

$$\begin{cases} z_1-\dot{g}_1(\lambda,\Delta V)\le s_1 \\ s_1\ge 0 \end{cases} \tag{32a}$$

$$\begin{cases} z_2-\dot{g}_2(\lambda,\Delta V)\le s_2 \\ s_2\ge 0 \end{cases} \tag{32b}$$

Then, the slack variables are added to the objective function, regarded as penalty terms, to tighten the relaxation.

Finally, the penalty convex-concave model for the hour-ahead VVC is given as:

$$\min\left(\omega\sum_{t\in T}\sum_{ij\in B}P_{ij,t}^{loss}+(1-\omega)\sum_{t\in T}V_t^{dev}+\pi^k\sum_{t\in T}\sum_{i\in I}(s_{1,i,t}+s_{2,i,t})\right) \tag{33a}$$

s.t.

$$\text{(2)-(3), (10)-(15), (17), (19)-(20), (22)-(23), (25a), (27)-(28), (31b), (31d), (32)} \tag{33b}$$

where π^k should increase as the iteration continues for convergence improvement [29].

D. CCP-based Solution Algorithm

A CCP-based solution algorithm is developed in this subsection to iteratively solve this penalty convex-concave model, as presented in Fig. 4.

The SOCR model provides a lower bound to the original hour-ahead problem, which can serve as an initial solution. Compared with the SOCR model, the feasible region of the penalty convex-concave model is the same. Due to the convexification of (31b), (31d), and the penalty terms, the objective function of (33) is non-increasing [29], providing an upper bound.

Accordingly, the following termination criteria are considered.

$$C1:\left|\frac{obj_0^k-obj_0^{k-1}}{obj_0^{k-1}}\right|\le\varphi_1 \tag{34a}$$

$$C2:\sum_{t\in T}\sum_{i\in I}(s_{1,i,t}+s_{2,i,t})\le\varphi_2 \tag{34b}$$

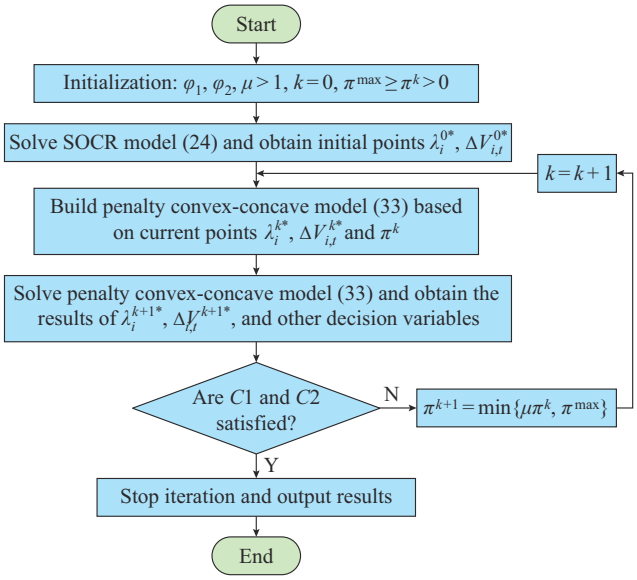

Fig. 4. CCP-based solution algorithm for solving penalty convex-concave model.

$C1$ determines the difference of the original objective function (24) between the current and last iterations, while $C2$ checks the sum of the slack variables to ensure equality constraints.

Note that the penalty convex-concave model is a second-order cone programming problem, which can be efficiently solved by off-the-shelf solvers. The logic and procedure of the solution algorithm for dealing with the bilinear constraints can also be applied to other practical optimization problems such as microgrid planning and operation.

V. Case Study on 33-bus Distribution Network

A. Test System

A 33-bus distribution network [37] with 10 PV units is applied to test the proposed method, as shown in Fig. 5. This network has been widely used in VVC [8], [18] and microgrid energy management [32] problems. The rated active power of PV units in the 33-bus distribution network is given in Table II. The PV inverter capacity is oversized by 10% such that about 45% capacity is available for reactive power compensation at the rated active power outputs of PV panels [4]. Besides, the PBDR settings can be referred to Table I. The predicted profiles of PV output and load before PBDR are given in Fig. 6, which represents the expected scenario. The predicted uncertainty intervals are set to be ±30% of the expected values for the PV generation and ±20% of the expected values for the loads. Then, 50 scenarios are generated with a uniform distribution [34], [38] inside the predicted uncertainty intervals to represent uncertainty realizations for the day-ahead stage. Similarly, 60 scenarios are generated to represent minute uncertainty realizations for the hour-ahead stage. Moreover, the allowed voltage range is set between 0.95 p.u. and 1.05 p.u.. Regarding the penalty CCP, tolerances φ_1 and φ_2 are set to be 0.001, and parameters π^0= 1, μ=4.

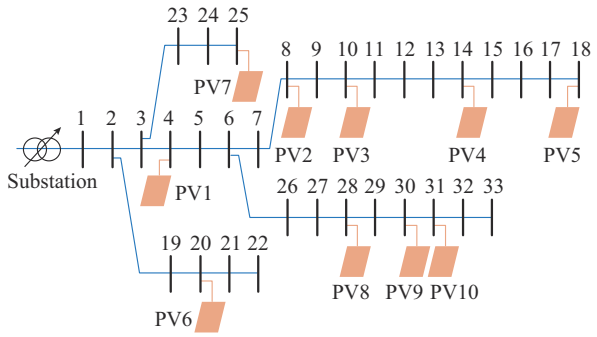

Fig. 5. 33-bus distribution network with 10 PV units.

TABLE II
RATED ACTIVE POWER OF PV UNITS IN 33-BUS DISTRIBUTION NETWORK

PV No.	Rated active power (kW)	PV No.	Rated active power (kW)
1	600	6	600
2	550	7	650
3	600	8	550
4	600	9	600
5	500	10	650

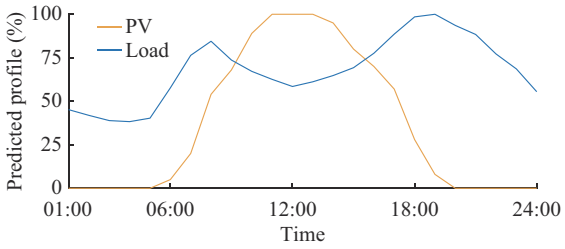

Fig. 6. Predicted profiles of PV output and load response before PBDR.

This numerical simulation is conducted on a 64-bit PC with a 2.5 GHz CPU and 16 GB RAM using YALMIP [39] interface on MATLAB platform. GUROBI solver [40] is used to solve the optimization problems.

B. Day-ahead PBDR Results

By solving the day-ahead PBDR-supported central voltage control model, the results of scheduled day-ahead PBDR price levels are obtained, as shown in Fig. 7. The load demand increases in response to the lower prices during period 02:00-06:00 and 08:00-17:00, and decreases in response to the higher price during period 18:00-23:00. From this point, PBDR, as an active power resource, can achieve load leveling and shifting, which in turn facilitates the microgrid operation. The average power loss and voltage deviation over the whole day are 3.453 MW and 0.0488 p.u., respectively.

Besides, it is worth noting that without the PBDR and inverter-based VVC, the voltage range under the expected condition is [0.92, 1.07]p.u., which is out of the allowed voltage range. However, with the coordination of PBDR and inverter reactive power supply, the voltage range under the expected condition is [0.99, 1.02]p.u., indicating a significant improvement in voltage deviation reduction.

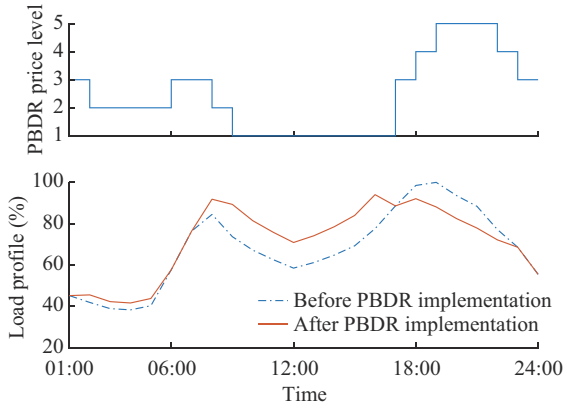

Fig. 7. Scheduled day-ahead PBDR price levels and expected load response.

C. Hour-ahead Hierarchically Coordinated VVC Results

The hour-ahead hierarchically coordinated VVC is solved by the proposed CCP-based solution algorithm. Since the voltage profile has been improved in the day-ahead stage, only power loss reduction is considered as the objective in the hour-ahead stage.

Taking the period of 12:00-13:00 as an example, the total expected PV generation and loads with PBDR implementation are 5.9 MW and 2.63 MW, respectively.

Figure 8 shows the solving process of the proposed CCP-based solution algorithm during this period. Except for the initial SOCR model (iteration 0), it takes 3 iterations to reach the termination criteria, showing a high convergence rate. The total solving time is 38.7 s, which is compatible for practical online applications.

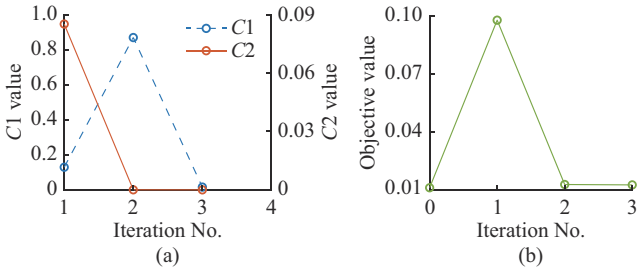

Fig. 8. Solving process of proposed CCP-based solution algorithm during period 12:00-13:00 in 33-bus distribution network. (a) $C1$ and $C2$ values. (b) Objective value.

By iteratively solving the hour-ahead penalty convex-concave model, the average power loss during this period is 125 kW. Note that since only power loss is considered in the hour-ahead stage, the results can achieve a better power loss reduction compared with that in the day-ahead stage.

Moreover, the results of reactive power setpoints Q_i^{set}, expected bus voltage V_i^{exp}, and the slope of droop control functions λ_i are obtained. Thus, the associated Q-V droop curves of the inverters with the reactive power setpoints can be plotted, as shown in Fig. 9. It shows that the reactive power setpoints of some PV inverters such as PV1, PV4, PV5, and PV9 reach the maximum inverter capacity for the reactive power. PV2-PV5 have negative reactive power setpoints

while other PV inverters have positive setpoints.

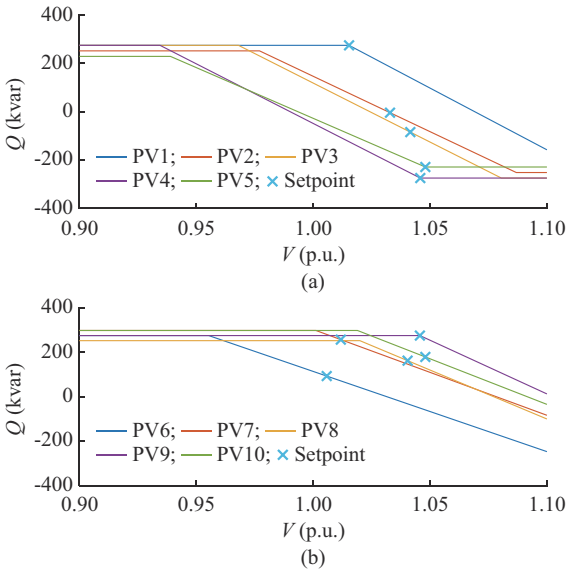

Fig. 9. *Q-V* droop curves of PV inverters with reactive power setpoints during period 12:00-13:00. (a) PV1-PV5. (b) PV6-PV10.

Besides, the *Q-V* droop curves of the PV inverters with the reactive power setpoints during the peak load period 20: 00-21: 00 are given in Fig. 10 for comparison. In this case, the PV generation is zero and the total load after PBDR is 3.06 MW. Since there is no active power generation, all PV inverters can make full use of their capacity for reactive power compensation with all positive setpoints. During this period, PV6 produces constant reactive power. The average power loss during this period is 81 kW, which is smaller than that observed around noon.

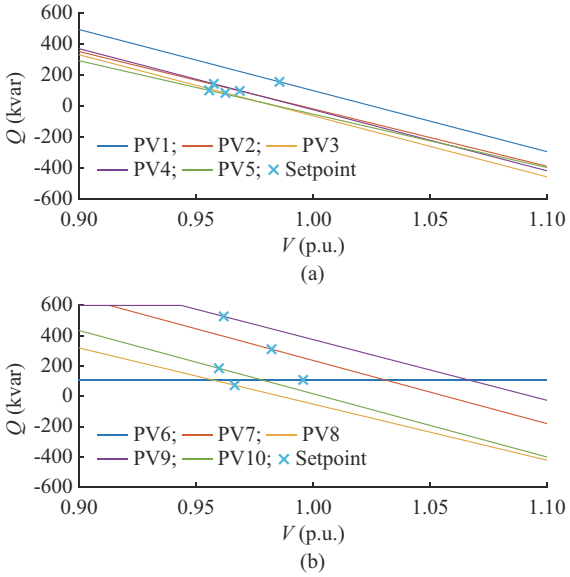

Fig. 10. *Q-V* droop curves of inverters with reactive power setpoints during period 20:00-21:00. (a) PV1-PV5. (b) PV6-PV10.

D. RT Local VVC and Comparison with Other Methods

In the RT stage, the inverters that operate under droop control mode can change the reactive power supply in response to the measurement of local bus voltage based on the optimized droop control function.

To verify the effectiveness of the droop control function and the proposed PBDR-supported three-stage HCVC method, 5000 scenarios of PV outputs and loads are randomly generated by Monte Carlo sampling during the periods 12: 00-13:00 and 20:00-21:00. These two periods correspond to the peak PV generation period and the peak load period, respectively, which can be regarded as two typical cases of the whole day. Then, 20% PV output scenarios are randomly selected and set to be 30% of the original value to simulate PV ramping events such as cloud passing. These scenarios are regarded as RT uncertainty realizations.

In addition, two other voltage control methods are applied for comparison, which are given as follows.

1) Method 1: HCVC without PBDR implementation. The inverter reactive power setpoint and droop control function are optimized every hour. Then, with local RT bus voltage measurement, each inverter changes its reactive power output based on the optimized droop control function.

2) Method 2: two-stage central coordination of PBDR and inverter reactive power generation without local control. The inverter reactive power dispatch is re-optimized every hour and fixed.

The comparison results during the periods 12: 00-13: 00 and 20:00-21:00 are given in Tables III and IV, respectively.

TABLE III
COMPARISON RESULTS OF DIFFERENT METHODS DURING PERIOD 12:00-13:00

Method	Average power loss (kW)	Voltage range (p.u.)	Voltage violation rate (%)
1	110.4	[0.997, 1.048]	0
2	95.8	[0.966, 1.044]	0
Proposed	80.0	[0.996, 1.045]	0

TABLE IV
COMPARISON RESULTS OF DIFFERENT METHODS DURING PERIOD 20:00-21:00

Method	Average power loss (kW)	Voltage range (p.u.)	Voltage violation rate (%)
1	105.3	[0.947, 0.998]	2.08
2	81.2	[0.949, 0.998]	0.12
Proposed	81.0	[0.953, 0.998]	0

During the peak PV generation period 12:00-13:00, Method 1 has the largest average power loss, followed by Method 2, indicating the significance of PBDR for power loss reduction. However, the voltage range of Method 2 is larger than that of Method 1, but both are within the allowed voltage range. For the proposed method, it obtains the lowest average power loss, and the voltage range is similar to that of Method 1. Also, all the methods have no voltage violations.

During the peak load period 20: 00-21: 00, the average power loss, voltage range, and voltage violation rate of Method 1 are the largest, indicating that only using inverter reactive power compensation cannot fully address the volt-

age issue. By contrast, the average power loss and voltage violation rate in Method 2 are greatly reduced due to the consideration of PBDR, but voltage violation still occurs. Regarding the proposed method, although its average power loss and voltage range are slightly less than those of Method 2, no voltage violations are observed.

In addition, based on the simulation results of 5000 scenarios, the probability distribution of the microgrid power loss during the period 12:00-13:00 for Method 2 and the proposed method is given in Fig. 11. It shows that the proposed method with local droop control can achieve a great power loss reduction. Note that because no PBDR is implemented, the load profile of Method 1 is obviously different from that of the other two methods, causing the power loss to be the largest. Thus, Fig. 11 is used to compare the performances of Method 2 and the proposed method in power loss reduction.

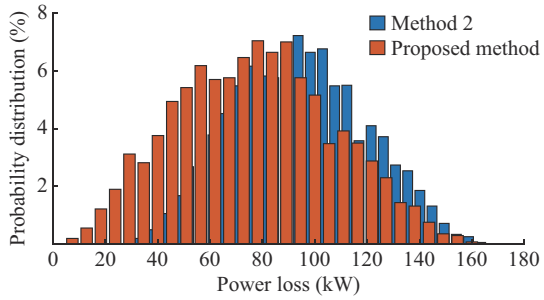

Fig. 11. Probability distribution of microgrid power loss during period 12:00-13:00 for Method 2 and proposed method.

Moreover, the probability distribution of the voltage profile at Bus 18 (end bus along feeder) during the period 20:00-21:00 for all methods are plotted in Fig. 12.

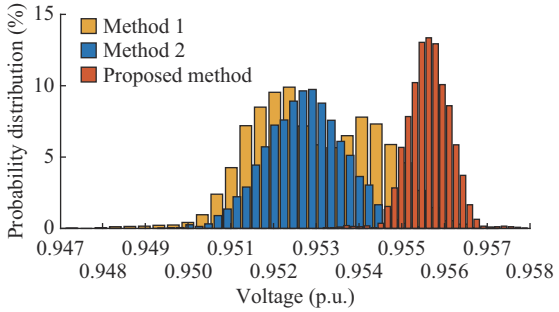

Fig. 12. Probability distribution of voltage profile at Bus 18 during period 20:00-21:00 for all methods.

As observed from this figure, Method 1 has the widest voltage range and largest voltage violation rate. The voltage profile of Method 2 is significantly improved compared with that of Method 1 due to the coordination of PBDR. For the proposed method, the bus voltage does not exceed the allowed range with a better voltage profile (further from the lower voltage limit) and less deviation range, showing superior performance in voltage regulation against uncertainties.

In summary, the above comparison shows the effectiveness of the PBDR as an active power resource to support voltage control. More importantly, the proposed method takes advantage of the central and local VVC methods with the load shifting function of PBDR, demonstrating the high efficiency for power loss reduction and voltage regulation.

VI. Case Study on IEEE 123-bus Distribution Network

A. Test System

This paper also applies the IEEE 123-bus distribution network [41] to verify the scalability of the proposed method. There are 14 PV units installed in the network and their locations are marked with red circles in Fig. 13. The rated active power of PV units in the IEEE 123-bus distribution network is given in Table V. Other settings are the same as those in the 33-bus system.

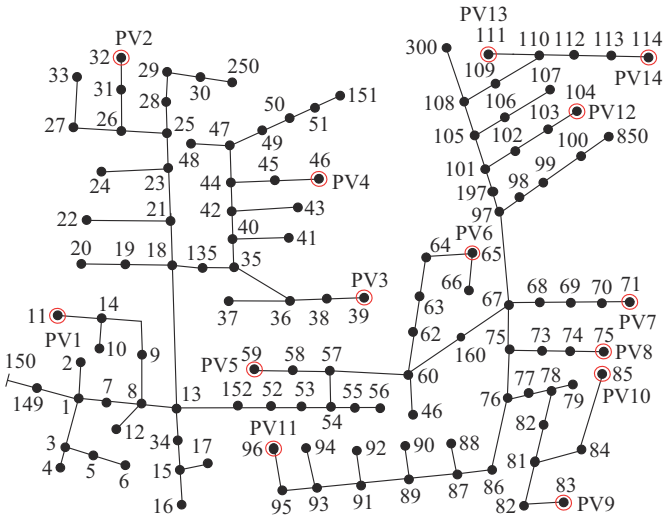

Fig. 13. IEEE 123-bus distribution network with 14 PV units.

TABLE V
Rated Active Power of PV Units in IEEE 123-bus Distribution Network

PV No.	PV rated power (kW)	PV No.	PV rated power (kW)
1	230	8	270
2	250	9	250
3	240	10	230
4	260	11	240
5	250	12	240
6	480	13	250
7	250	14	230

B. Day-ahead and Intraday Simulation Results

The load profiles before and after PBDR implementation are obtained by solving the day-ahead PBDR-supported central voltage control model, which is shown in Fig. 14. The load demand increases from 09:00 to 16:00 when the scheduled PBDR price levels are lower, while it decreases from 18:00 to 22:00 when the price levels are higher. The estimated average power loss and voltage deviation of the entire day are 683.4 kW and 0.073 p.u., respectively.

During the entire day, the proposed CCP-based solution algorithm is used to solve the hour-ahead hierarchically coordi-

nated VVC. Similarly, taking the peak PV generation period 12:00-13:00 as an example, the total expected PV generation and load demand after PBDR are 3.67 MW and 2.58 MW, respectively. The solving process of the CCP-based solution algorithm is shown in Fig. 15. The SOCR model is solved first (iteration 0) to provide the initial solution. Then, the other 3 iterations are taken to obtain the results. The solving time is 57.6 s, indicating that the proposed CCP-based solution algorithm is suitable for online use even in the larger system. During this period, the power loss is 27.4 kW and the voltage deviation is 0.0027 p.u..

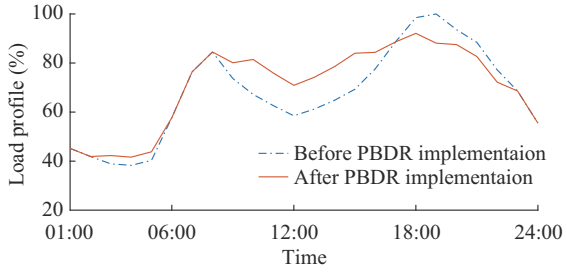

Fig. 14. Load profiles before and after PBDR implementation of IEEE 123-bus distribution network.

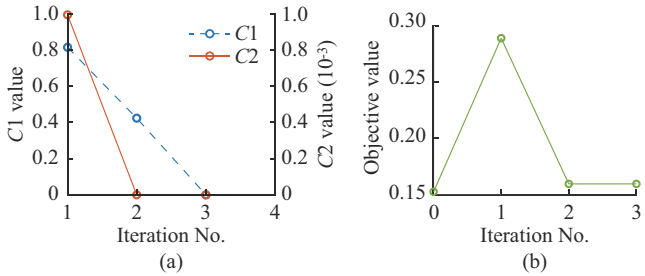

Fig. 15. Solving process of proposed CCP-based solution algorithm during period 12:00-13:00 in IEEE 123-bus distribution network. (a) $C1$ and $C2$ values. (b) Objective value.

C. RT Local VVC and Comparison with Other Methods in IEEE 123-bus Distribution Network

To further verify the effectiveness of the proposed method as well as the optimized droop control function in the IEEE 123-bus distribution network, 5000 scenarios of PV outputs and loads during the periods 12:00-13:00 and 20:00-21:00 are randomly generated using the same setting of the 33-bus distribution network in Section V-D. Moreover, Methods 1 and 2 in Section V-D are adopted for comparison. The comparison results of average power loss and voltage range during these two periods are given in Tables VI and VII, respectively.

TABLE VI
COMPARISON RESULTS OF DIFFERENT METHODS DURING PERIOD 12:00-13:00 IN IEEE 123-BUS DISTRIBUTION NETWORK

Method	Average power loss (kW)	Voltage range (p.u.)
1	25.73	[0.984, 1.015]
2	21.28	[0.980, 1.018]
Proposed	20.58	[0.984, 1.015]

TABLE VII
COMPARISON RESULTS OF DIFFERENT METHODS DURING PERIOD 20:00-21:00 IN IEEE 123-BUS DISTRIBUTION NETWORK

Method	Average power loss (kW)	Voltage range (p.u.)
1	58.61	[0.990, 1.005]
2	52.63	[0.990, 1.006]
Proposed	52.37	[0.993, 1.005]

During the peak PV generation period 12:00-13:00, the average power loss of Method 1 is significantly higher than that of Method 2 and the proposed method, indicating that PBDR is effective in reducing network loss. However, the voltage range of Method 2 becomes wider compared with that of Method 1, but both are within the allowed voltage range. Lastly, the proposed method can achieve the lowest average power loss and the smallest voltage range, indicating the effectiveness of the optimized droop control function in the hour-ahead stage.

During the peak load period 20:00-21:00, Method 1 has the largest average power loss, while the power loss of Method 2 significantly decreases after PBDR implementation. The proposed method achieves the smallest average power loss as well as voltage range.

It is worth noting that during these two periods, all the methods do not encounter the violation of voltage constraints.

With the results of these 5000 scenarios, the probability distribution of the voltage of phase C at Bus 31 during the period 12:00-13:00 for all the methods are plotted in Fig. 16. As shown in this figure, the voltage profile of Method 1 without PBDR is generally larger than that of the other two methods. Compared with Method 2, the proposed method greatly reduces the voltage deviation, making the bus voltage closer to the reference bus voltage of 1 p.u..

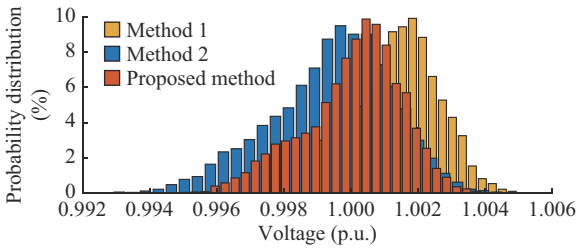

Fig. 16. Probability distribution of voltage of phase C at Bus 31 during period 12:00-13:00.

In addition, the probability distribution of microgrid power loss during the period 20:00-21:00 for Method 2 and the proposed method are given in Fig. 17. The microgrid power loss of the proposed method is generally lower than that of Method 2, which shows the high efficiency of optimized droop control function in the voltage regulation.

In summary, the above comparison shows the superiority of the proposed method in microgrid power loss reduction and voltage control.

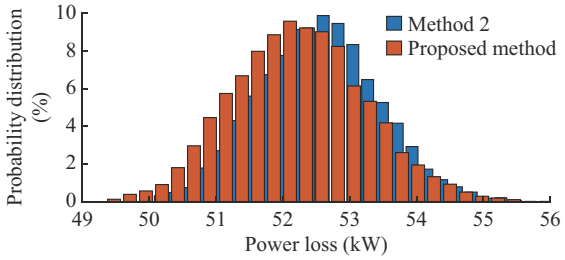

Fig. 17. Probability distribution of microgrid power loss during period 20:00-21:00.

VII. Conclusion

In this paper, a PBDR-supported three-stage HCVC method is introduced, aiming to minimize the microgrid power loss and voltage deviation via co-optimizing the operation of both active and reactive power resources. The day-ahead PBDR scheduling is efficiently coordinated with intraday inverter reactive power dispatch in a centralized manner via a SO method. By contrast, the inverter reactive power dispatch and RT local control are hierarchically coordinated considering the possible RT uncertainty scenarios.

Several linearization methods are applied to solve the nonlinear constraints for the day-ahead model. Then, in the second-stage hierarchical VVC, to exploit the PV inverter potentials, the reactive power output is considered to be constant or adjustable based on a linear *Q-V* droop control function. The key parameters of the droop control function, which include the droop slope and a pair of base coordinates representing the expected voltage and corresponding reactive power setpoint, are fully modelled. More importantly, a CCP-based solution algorithm including model relaxation, reformulation, and solving procedure is developed to efficiently solve the second-stage optimization problem. The case study verifies the effectiveness and high efficiency of the proposed method and solution algorithm.

The proposed method focuses on the coordination of PBDR and PV inverters. However, there are various distributed energy resources and network devices such as battery energy storage and CBs in microgrids. In future research works, the proposed method can be expanded to coordinate with these resources and devices. Moreover, a more general model of the droop control function with deadband and the three-phase unbalance issue of the microgrid can be considered.

References

[1] B. Wang, C. Zhang, Z. Y. Dong *et al*., "Improving hosting capacity of unbalanced distribution networks via robust allocation of battery energy storage systems," *IEEE Transactions on Power Systems*, vol. 36, no. 3, pp. 2174-2185, May 2021.

[2] C. Zhang and Y. Xu, "Hierarchically-coordinated voltage/var control of distribution networks using PV inverters," *IEEE Transactions on Smart Grid*, vol. 11, no. 4, pp. 2942-2953, Jul. 2020.

[3] X. Chen, "Green and low-carbon energy-use," *The Innovation Energy*, vol. 1, no. 1, p. 100003, Feb. 2024.

[4] C. Zhang, Y. Xu, Z. Dong *et al*., "Three-stage robust inverter-based voltage/var control for distribution networks with high-level PV," *IEEE Transactions on Smart Grid*, vol. 10, no. 1, pp. 782-793, Jan. 2019.

[5] Y. Zhang, Y. Xu, H. Yang *et al*., "Voltage regulation-oriented co-planning of distributed generation and battery storage in active distribution networks," *International Journal of Electrical Power & Energy Systems*, vol. 105, pp. 79-88, Feb. 2019.

[6] *IEEE Standard for Interconnection and Interoperability of Distributed Energy Resources with Associated Electric Power Systems Interfaces*, IEEE Std 1547-2018 (Revision of IEEE Std 1547-2003), 2018.

[7] F. U. Nazir, B. Pal, and R. Jabr, "A two-stage chance constrained volt/var control scheme for active distribution networks with nodal power uncertainties," in *Proceedings of 2019 IEEE PES General Meeting*, Atlanta, USA, Jan. 2019, pp. 314-325.

[8] Z. Wang, W. Tan, H. Li *et al*., "A voltage coordination control strategy based on the reactive power-active network loss partitioned aggregation domain," *International Journal of Electrical Power & Energy Systems*, vol. 144, p. 108585, Jan. 2023.

[9] F. Ding and B. Mather, "On distributed PV hosting capacity estimation, sensitivity study, and improvement," *IEEE Transactions on Sustainable Energy*, vol. 8, no. 3, pp. 1010-1020, Jul. 2017.

[10] F. Capitanescu, L. F. Ochoa, H. Margossian *et al*., "Assessing the potential of network reconfiguration to improve distributed generation hosting capacity in active distribution systems," *IEEE Transactions on Power Systems*, vol. 30, no. 1, pp. 346-356, Jan. 2015.

[11] G. Tapia-Tinoco, D. Granados-Lieberman, M. Valtierra-Rodriguez *et al*., "Modeling of electric springs and their multi-objective voltage control based on continuous genetic algorithm for unbalanced distribution networks," *International Journal of Electrical Power & Energy Systems*, vol. 138, p. 107979, Jun. 2022.

[12] A. Singhal, V. Ajjarapu, J. Fuller *et al*., "Real-time local volt/var control under external disturbances with high PV penetration," *IEEE Transactions on Smart Grid*, vol. 10, no. 4, pp. 3849-3859, Jul. 2019.

[13] K. Turitsyn, P. Sulc, S. Backhaus *et al*., "Options for control of reactive power by distributed photovoltaic generators," *Proceedings of the IEEE*, vol. 99, no. 6, pp. 1063-1073, Jun. 2011.

[14] C. Zhang, Y. Xu, Y. Wang *et al*., "Three-stage hierarchically-coordinated voltage/var control based on PV inverters considering distribution network voltage stability," *IEEE Transactions on Sustainable Energy*, vol. 13, no. 2, pp. 868-881, Apr. 2022.

[15] H. Sekhavatmanesh, G. Ferrari-Trecate, and S. Mastellone, "Optimal adaptive droop design via a modified relaxation of the OPF," *IEEE Transactions on Control Systems Technology*, vol. 31, no. 2, pp. 497-510, Mar. 2023.

[16] F. Sun, J. Ma, M. Yu *et al*., "Optimized two-time scale robust dispatching method for the multi-terminal soft open point in unbalanced active distribution networks," *IEEE Transactions on Sustainable Energy*, vol. 12, no. 1, pp. 587-598, Jan. 2021.

[17] P. Li, Z. Wu, C. Zhang *et al*., "Multi-timescale affinely adjustable robust reactive power dispatch of distribution networks integrated with high penetration of PV," *Journal of Modern Power Systems and Clean Energy*, vol. 11, no. 1, pp. 324-334, Jan. 2023.

[18] R. Xu, C. Zhang, Y. Xu *et al*., "Multi-objective hierarchically-coordinated volt/var control for active distribution networks with droop-controlled PV inverters," *IEEE Transactions on Smart Grid*, vol. 13, no. 2, pp. 998-1011, Mar. 2022.

[19] A. Savasci, A. Inaolaji, and S. Paudyal, "Two-stage volt-var optimization of distribution grids with smart inverters and legacy devices," *IEEE Transactions on Industry Applications*, vol. 58, no. 5, pp. 5711-5723, Sept. 2022.

[20] A. Savasci, A. Inaolaji, and S. Paudyal, "Optimal droop scheduling of smart inverters in unbalanced distribution feeders," in *Proceedings of 2023 IEEE PES General Meeting*, Orlando, USA, Jul. 2023, pp. 1-5.

[21] D. Liu, C. Zhang, Y. Xu *et al*., "Sensitivity region-based optimization for maximizing renewable generation hosting capacity of an islanded microgrid," *IEEE Transactions on Smart Grid*, vol. 14, no. 4, pp. 2496-2507, Jul. 2023.

[22] Y. Liu, Z. Li, and J. Zhao, "Safety-constrained stagewise optimization of droop control parameters for isolated microgrids," *IEEE Transactions on Smart Grid*, vol. 15, no. 1, pp. 77-88, Jan. 2024.

[23] U.S. Department of Energy, "Benefits of demand response in electricity markets and recommendations for achieving them. A report to the United States Congress pursuant to section 1252 of the Energy Policy Act of 2005", U.S. Dept. Energy, Washington DC, USA, Tech. Rep., 2006.

[24] C. Zhang, Y. Xu, Z. Y. Dong *et al*., "Robust coordination of distributed generation and price-based demand response in microgrids," *IEEE Transactions on Smart Grid*, vol. 9, no. 5, pp. 4236-4247, Sept. 2018.

[25] H. Hua, X. Chen, L. Gan *et al*., "Demand-side joint electricity and carbon trading mechanism," *IEEE Transactions on Industrial Cyber-Physical Systems*, vol. 2, pp. 14-25, Nov. 2024.

[26] B. Wang, C. Zhang, and Z. Y. Dong, "Interval optimization based coordination of demand response and battery energy storage system con-

sidering SOC management in a microgrid," *IEEE Transactions on Sustainable Energy*, vol. 11, no. 4, pp. 2922-2931, Oct. 2020.
[27] S. He, H. Gao, H. Tian *et al*., "A two-stage robust optimal allocation model of distributed generation considering capacity curve and real-time price based demand response," *Journal of Modern Power Systems and Clean Energy*, vol. 9, no. 1, pp. 114-127, Jan. 2021.
[28] Y. Wang, X. Ai, Z. Tan *et al*., "Interactive dispatch modes and bidding strategy of multiple virtual power plants based on demand response and game theory," *IEEE Transactions on Smart Grid*, vol. 7, no. 1, pp. 510-519, Jan. 2016.
[29] T. Lipp and S. Boyd, "Variations and extension of the convex-concave procedure," *Optimization and Engineering*, vol. 17, no. 2, pp. 263-287, Jun. 2016.
[30] P. R. Thimmapuram, J. Kim, A. Botterud *et al*., "Modeling and simulation of price elasticity of demand using an agent-based model," in *Proceedings of 2010 Innovative Smart Grid Technologies*, Gaithersburg, USA, Jan. 2010, pp. 1-8.
[31] H. G. Yeh, D. F. Gayme, and S. H. Low, "Adaptive var control for distribution circuits with photovoltaic generators," *IEEE Transactions on Power Systems*, vol. 27, no. 3, pp. 1656-1663, Aug. 2012.
[32] B. Wang, C. Zhang, C. Li *et al*., "Transactive energy sharing in a microgrid via an enhanced distributed adaptive robust optimization approach," *IEEE Transactions on Smart Grid*, vol. 13, no. 3, pp. 2279-2293, May 2022.
[33] Y. Chen, X. Feng, Z. Li *et al*., "Multi-stage coordinated operation of a multi-energy microgrid with residential demand response under diverse uncertainties," *Energy Conversion and Economics*, vol. 1, no. 1, pp. 20-33, Oct. 2020.
[34] Z. Shi, Y. Xu, D. Xie *et al*., "Optimal coordination of transportable power sources and repair crews for service restoration of distribution networks considering uncertainty of traffic congestion," *Journal of Modern Power Systems and Clean Energy*, vol. 12, no. 1, pp. 189-201, Jan. 2024.
[35] G. P. McCormick, "Computability of global solutions to factorable nonconvex programs: part I – convex underestimating problems," *Mathematical Programming*, vol. 10, no. 1, pp. 147-175, Dec. 1976.
[36] A. L. Yuille and A. Rangarajan, "The concave-convex procedure," *Neural Computation*, vol. 15, no. 4, pp. 915-936, Apr. 2003.
[37] M. E. Baran and F. Wu, "Network reconfiguration in distribution systems for loss reduction and load balancing," *IEEE Transactions on Power Delivery*, vol. 4, no. 2, pp. 1401-1407, Apr. 1989.
[38] L. Gan, T. Yang, B. Wang *et al*., "Three-stage coordinated operation of steel plant-based multi-energy microgrids considering carbon reduction," *Energy*, vol. 278, p. 127639, Sept. 2023.
[39] J. Lofberg, "YALMIP: a toolbox for modeling and optimization in MATLAB," in *Proceedings of 2004 IEEE International Conference on Robotics and Automation*, Taipei, China, Sept. 2004, pp. 284-289.
[40] Gurobi. (2024, May). Gurobi 11.0. [Online]. Available: https://www.gurobi.com
[41] IEEE. (2024, May). IEEE distribution test feeders. [Online]. Available: https://site.ieee.org/pes-testfeeders/resources/

Bo Wang received the B.E. (hons.) degree in electrical engineering, the M.Eng.Sc. degree in energy system, and the Ph.D. degree in electrical engineering from the University of New South Wales (UNSW), Sydney, Australia, in 2013, 2014, and 2022, respectively. He is currently a Lecturer with the School of Electrical and Power Engineering, Hohai University, Nanjing, China. His research interests include planning and operation of distribution network and microgrid, transactive energy, energy-use net, and applications of optimization theory and machine learning.

Cuo Zhang received the B.E. (hons.) degree in electrical (power) engineering from the University of Sydney, Sydney, Australia, in 2014, and the Ph.D. degree in electrical engineering from the University of New South Wales, Sydney, Australia, in 2018. He is a Lecturer in power engineering with the University of Sydney. He is also a Discovery Early Career Researcher Award (DECRA) Fellow of Australian Research Council (ARC). His research interests include power system planning and operation, voltage stability and control, transactive energy, distributed energy resources, microgrid, and applications of optimization theory and artificial intelligence in these areas.

Xingying Chen received the B.Eng. and Ph.D. degrees from Southeast University, Nanjing, China, in 1984 and 2002, respectively, and an M.Eng. degree from Hohai University, Nanjing, China, in 1995, all in electrical engineering. She joined the faculty of Hohai University in 1984, and has become a Full Professor there since 2002. Her current research interests include distribution and utilization system of electric power, electricity market, energy management and control, energy economics, and energy-use net.

Yan Xu received the B.E. and M.E degrees from South China University of Technology, Guangzhou, China, in 2008 and 2011, respectively, and the Ph.D. degree from University of Newcastle, Newcastle, Australia, in 2013. After the postdoctoral training funded by University of Sydney Postdoctoral Fellowship, he joined Nanyang Technological University (NTU), Singapore, with the Nanyang Assistant Professorship. He was promoted to Associate Professor in early 2021 and appointed as the Cham Tao Soon Professor in Engineering (an endowed professorship named after NTU's founding president) in early 2024. At NTU, he concurrently serves as the Director of Center for Power Engineering (CPE), and Co-director of Singapore Power Group – NTU Joint Lab. His research interests include power system stability and control, microgrid, and data-analytics for smart grid applications.

Kun Yu received the B.Eng. and M.Eng. degrees from Hohai University, Nanjing, China, in 2000 and 2003, respectively, and the Ph.D. degree from Zhejiang University, Hangzhou, China, in 2011, all in electrical engineering. He joined the faculty of Hohai University in 2003, and has become a Full Professor there since 2023. His current research interests include self-healing control and optimal dispatching of smart distribution networks, efficient operation of energy-use system and energy economy, and energy-use net.

Haochen Hua received the B.Sc. degree in mathematics with finance in 2011, and the Ph.D. degree in mathematical sciences in 2016, both from the University of Liverpool, Liverpool, U.K. From 2016 to 2020, he was a Postdoctoral Fellow with the Research Institute of Information Technology, Tsinghua University, Beijing, China. Since 2020, he has been a Professor with the School of Electrical and Power Engineering, Hohai University, Nanjing, China. He has been the Chief Scientist of National Key R&D Program since 2023. His current research interests include energy-use net, energy management and control, energy economics, and stochastic optimal and robust control theory.

Zhao Yang Dong is a Chair Professor and the Head of Department of Electrical Engineering, City University of Hong Kong, Hong Kong, China. His immediate role is SPG Endowed Professor of Power Engineering, and Co-director of SPG-NTU Joint Lab at Nanyang Technological University, Singapore. His previous roles include SHARP Professor and the inaugural Director of University of New South Wales (UNSW) Digital Grid Futures Institute, Sydney, Australia; Director of ARC Research Hub for Integrated Energy Storage Solutions; Ausgrid Chair Professor and Director of Ausgrid Centre for Intelligent Electricity Networks providing R&D support for the AU $500m Smart Grid, Smart City National Demonstration Project of Australia. His research interests include power system planning, load modelling, smart grid, smart city, energy market, renewable energy and its grid connection, and computational methods and their application in power system analysis.